molecules

MDPI

Article

Highly Efficient Methylene Blue Dye Removal by Nickel Molybdate Nanosorbent

Souad Rakass [1,*], Hicham Oudghiri Hassani [2], Ahmed Mohmoud [3,4], Fethi Kooli [5], Mostafa Abboudi [4], Eman Assirey [4] and Fahd Al Wadaani [4]

1 Laboratory of Applied Organic Chemistry (LCOA), Chemistry Department, Faculty of Sciences and Techniques, Sidi Mohamed Ben Abdellah University, Imouzzer Road, P.O. Box 2202, 30000 Fez, Morocco
2 Engineering Laboratory of Organometallic, Molecular Materials and Environment (LIMOME), Faculty of Sciences, Chemistry Department, Sidi Mohamed Ben Abdellah University, P.O. Box 1796 (Atlas), 30000 Fez, Morocco; oudghiri_hassani_hicham@yahoo.com
3 Petroleum Technology, Operated Offshore Oil Field Development, Qatar Petroleum, P.O. Box 3212, Doha, Qatar; caadil77@yahoo.co.uk
4 Chemistry Department, College of Science, Taibah University, Al-Madinah Al-Munawwarah 30002, Saudi Arabia; abboudi14@hotmail.com (M.A.); eman_assirey@hotmail.com (E.A.); fwadaani@taibahu.edu.sa (F.A.W.)
5 Department of Chemistry, Faculty of Science, Islamic University of Madinah, Al-Madinah Al-Munawwarah 42351, Saudi Arabia; fethi_kooli@yahoo.com
* Correspondence: rakass_souad@yahoo.fr; Tel.: +212-6449950091

Abstract: Removing methylene blue (MB) dye from aqueous solutions was examined by the use of nickel molybdate (α-$NiMoO_4$) as an adsorbent produced by an uncomplicated, rapid, and cost-effective method. Different results were produced by varying different parameters such as the pH, the adsorbent dose, the temperature, the contact time, and the initial dye concentration. Adsorbent dose and pH had a major removal effect on MB. Interestingly, a lower amount of adsorbent dose caused greater MB removal. The amount of removal gained was efficient and reached a 99% level with an initial methylene blue solution concentration of $\leq$160 ppm at pH 11. The kinetic studies indicated that the pseudo-second-order kinetic model relates very well with that of the obtained experimental results. The thermodynamic studies showed that removing the MB dye was favorable, spontaneous, and endothermic. Impressively, the highest quantity of removal amount of MB dye was 16,863 mg/g, as shown by the Langmuir model. The thermal regeneration tests revealed that the efficiency of removing MB (11,608 mg/g) was retained following three continuous rounds of recycled adsorbents. Adsorption of MB onto α-$NiMoO_4$ nanoparticles and its regeneration were confirmed by Fourier transform infrared spectroscopy (FTIR) analysis and scanning electron microscopy (SEM) analysis. The results indicated that α-$NiMoO_4$ nanosorbent is an outstanding and strong candidate that can be used for removing the maximum capacity of MB dye in wastewater.

Keywords: nanosorbent; regeneration; α-$NiMoO_4$; methylene blue; removal

check for updates

Citation: Rakass, S.; Oudghiri Hassani, H.; Mohmoud, A.; Kooli, F.; Abboudi, M.; Assirey, E.; Al Wadaani, F. Highly Efficient Methylene Blue Dye Removal by Nickel Molybdate Nanosorbent. *Molecules* **2021**, *26*, 1378. https://doi.org/10.3390/molecules26051378

Academic Editors: Chiara Bisio and Monica Pica

Received: 31 December 2020
Accepted: 27 February 2021
Published: 4 March 2021

Publisher's Note: MDPI stays neutral with regard to jurisdictional claims in published maps and institutional affiliations.

Copyright: © 2021 by the authors. Licensee MDPI, Basel, Switzerland. This article is an open access article distributed under the terms and conditions of the Creative Commons Attribution (CC BY) license (https://creativecommons.org/licenses/by/4.0/).

1. Introduction

Dyes have recently been extensively utilized in several industrial and manufacturing applications, e.g., printing, textile, paper, carpet, and cosmetics. Dyes are considered toxic, hazardous pollutants and require removal before their discharge into the environment [1–7].

Numerous methods have been developed for dye removal from wastewater and industrial waste matter, including adsorption, coagulation, photodegradation, flocculation, membrane separation, ion exchange, biological treatment, chemical oxidation, and extraction [8–15].

Adsorption application is extensively employed due to its ease of process and guarantee of superb minimal cost from among those above-mentioned methods [1,16–21]. Several natural adsorbents have been successful in the elimination of color from aqueous waste

matter [22–25]. A universally used example is activated carbon owing to the presence of its large surface area [26,27]. There are still some difficulties that limit its use, such as its high cost of production, low-quality mechanical properties, regeneration issues, and phase separation strain [28]. The challenge faced by the researchers is to develop novel adsorbents with boundless adsorption capabilities that are capable of being regenerated for the recovery of reusable compounds.

In recent years, researchers have shown a great interest in binary metal oxides due to their potential performances for different materials [29]. In recent years, scientists have paid extensively studied the group of metal molybdates which has given the most favorable examples of mixed metal oxides [30–33]. Nickel molybdate ($NiMoO_4$) has various applications in catalysis such as hydrodesulfurization and hydrodenitrogenation reactions [34,35], oxidative dehydrogenation of light alkanes [36–40], partial oxidation of hydrocarbons [41], and microwave applications [42]. It is also used in humidity sensors [43], supercapacitors [44,45], optical fibers, and military devices [46]. Nickel molybdate has attractive structures and electrochemical and magnetic properties [47,48], and it can be found in two crystalline forms, α-$NiMoO_4$ and β-$NiMoO_4$.

Various methods of $NiMoO_4$ synthesis have been presented in the literature, including sonochemical [49,50], hydrothermal [46,51,52], precipitation [53,54], sol–gel [53], mechanochemical synthesis [55], solid state at high temperature [56,57], and microwave-assisted methods [58].

Recently, molybdate compounds have attracted great interest for their utilization in environmental applications such as the photocatalytic oxidation of dyes [59–62], the oxidation of methylene blue (MB) dye [63], and the sorption of water-soluble dyes [30,61].

In particular, α-$NiMoO_4$ synthesized by the microwave-assisted method has shown good photocatalytic activity for methylene blue photodegradation [58]. In addition, $NiMoO_4$ nanostructures synthesized by the coprecipitation method were efficiently used as a catalyst for methyl orange photooxidation under UV irradiation [64]. Furthermore, hydrothermally synthesized β-$NiMoO_4$ was recently used as a sono-photocatalyst for the degradation of methylene blue (MB) under diffused sunlight [65]. However, α-$NiMoO_4$ has not yet been explored for the removal of dyes by adsorption.

In the present work, nickel molybdate nanoparticles, synthesized using a facile and easy method without the use of any solvents, were evaluated for removing methylene blue dye (MB) as adsorbents. MB dye was utilized as an ideal dye owing to its extensive manufacturing uses as a food coloring agent and for cotton, wool, silk, and leather, to name a few examples [60]. The influence of diverse parameters, namely solution pH, initial concentration, adsorbent dose, and contact time, on the removal of methylene blue by synthesized α-$NiMoO_4$ nanosorbents was examined. The kinetics and adsorption isotherms were evaluated. In addition, after the nanosorbent had been regenerated by calcinating at high temperature, the removal efficiency was likewise investigated.

2. Results and Discussion

2.1. Removal of MB

2.1.1. pH Point of Zero Charge (pH_{pzc})

The pH point of zero charge (pH_{pzc}) can provide information regarding the surface charge of a material. The results found for this parameter are given in Figure 1. In fact, the pH_{pzc} of nickel molybdate was determined from graphs where the initial pH is equal to the final pH (intersection of curves). As shown in Figure 1, the nickel molybdate presented a surface charged negatively (pH_{pzc} = 8.96). The surface of nickel molybdate became negatively charged for a pH of solutions >8.96 and acquired a positive charge when the pH was lower than 8.96. According to the literature, the cation uptake is favorable at a pH > pH_{pzc}, whereas the uptake of anions is encouraged at a pH < pH_{pzc} of sorbent [66]. The obtained pH point of zero charge value is close to those obtained for some metal oxides such as CuO and NiO, which are in the range of 9–10 [67].

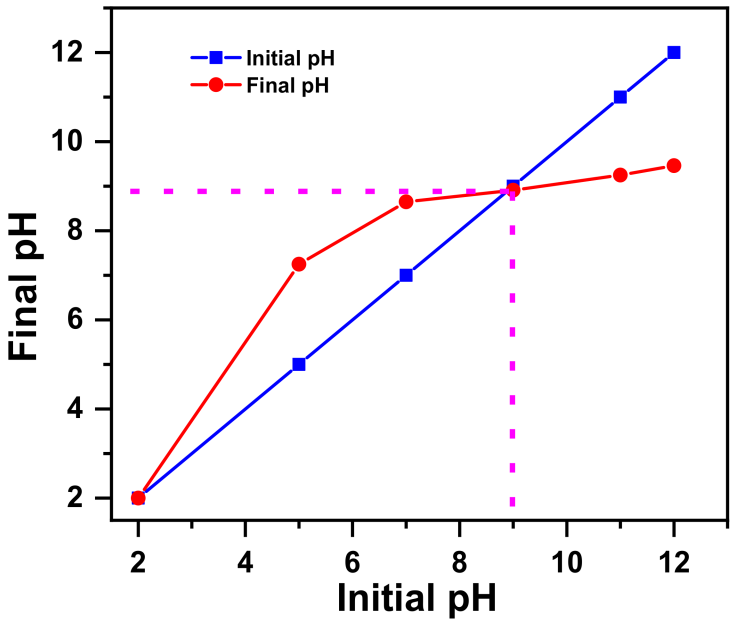

Figure 1. pH_{pzc} for nickel molybdate.

2.1.2. Effect of pH

pH is essential in terms of controlling the removal of dyes. It has no effect on altering the separation of the adsorbent site; nevertheless, it modifies the structure and the chemistry of the dye [68]. Moreover, the charge and surface potential of the oxide are primarily pH-dependent. It is possible, in some cases, to adjust the pH conditions of the slurry in such a way that all the particles exhibit the same charge polarity [68]. Hence, the effect of pH on the removal of MB by nickel molybdate (α-$NiMoO_4$) nanosorbent was assessed by varying pH values between 3 and 11 at a controlled temperature of 20 °C with the initial concentration of 100 ppm. Figure 2 demonstrates that methylene blue removal depended on the effect of pH. By increasing the pH from 3 to 7, the removal percentage did not substantially change and remained at about 29%. The further increase of pH to 9 slightly increased the removal percentage to 35%. The increase of pH to 11 led to the highly efficient removal of MB, as the removal percentage reached 93%. Moreover, there was an increase in the quantity of dye eliminated for every unit mass of the adsorbent at its equilibrium (qe) from 25 to 93 mg/g.

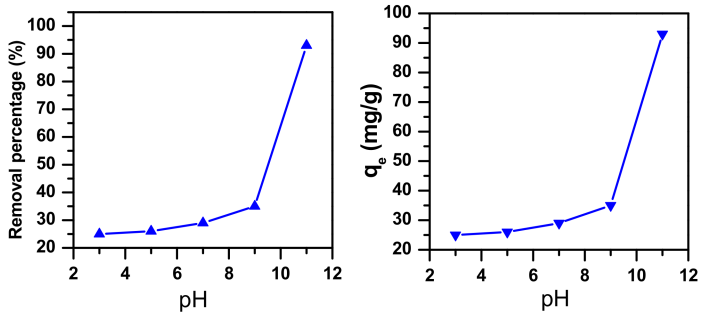

Figure 2. Effect of pH on dye removal performance of α-$NiMoO_4$ in a 100 ppm methylene blue solution (m_{ads} = 0.1 g, T = 20 °C, t = 30 min).

Strong electrostatic interactions took place between the charges of the MB dyes and those of α-$NiMoO_4$ adsorbent, as demonstrated by the increase in removal percentage obtained with the increase of the pH values. Furthermore, in the solution at pH 11, the hydroxyl group (OH^-) favors the direction of the positively charged MB as the pKa equals

3.8 [69]. Nevertheless, the lower removal performance at acidic values may well be related to the extra proton ions within the solution which are in concurrency with those of the basic dye cations on the removal sites of α-$NiMoO_4$. Comparable outcomes were reported by Kooli et al. in the examination of waste bricks utilized as favorable agents for the removal of basic blue 41 from liquid solutions [70].

On the other hand, these results can be explained by the point of zero charge value measured for nickel molybdate (pH_{pzc} = 8.96). The literature reports that at lower pH (pH < pH_{pzc}), the surface charge may become positive, thus allowing H^+ ions to compete effectively with dye cations and causing a decrease in the amount of dye adsorbed [71]. At higher pH (pH > pH_{pzc}), the nickel molybdate may become negatively charged, which enhances the positively charged cationic dye through electrostatic forces of attraction.

Thus, pH 11 was found to be the best value for the removal of MB when employing α-$NiMoO_4$ nanosorbent.

2.1.3. Effect of Adsorbent Dose

One crucial parameter in adsorption processes is the adsorbent dose [72]. The MB dye removal using α-$NiMoO_4$ was explored with varying adsorbent doses of 0.001 to 0.5 g/L with an initial dye concentration of 160 ppm. As can be seen clearly in Figure 3, the percentage (%) and the amount (mg/g) of MB removed were reduced as the nanosorbent dose increased from 0.001 to 0.5 g/L. The decrease in the removal effectiveness might be due to the performance of particle interaction (e.g., aggregation) as a result of the high dosage of the adsorbent. Such aggregation could increase diffusional path duration. Furthermore, the adsorption sites remain unsaturated throughout the course of sorption under these conditions. In fact, all of these factors can lead to a decrease in available particle size [73,74].

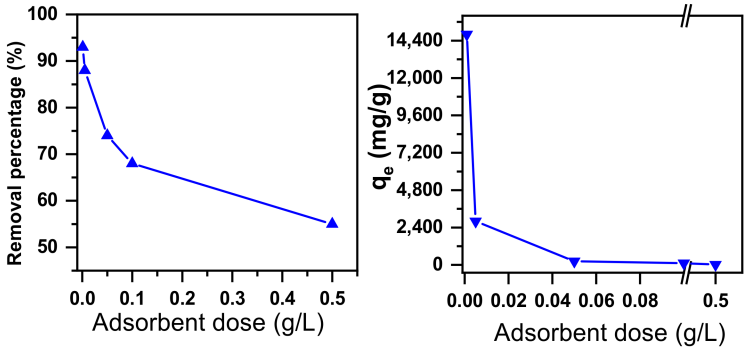

Figure 3. Effect of adsorbent dose on the dye removal performance of α-$NiMoO_4$ in a 160 ppm methylene blue solution (t = 30 min, T = 20 °C).

2.1.4. Effects of Initial Concentration and Contact Time

Figure 4 presents the effects of initial MB dye concentration and contact time on dye removal. The removal of MB was enhanced with the increase in contact time, reaching the highest value of 98% at around 30 min for initial methylene blue concentrations of 100 ppm. For MB concentrations of 120, 140, and 160 ppm, a maximum value of 99% removal was reached at around 60 min. However, the removal percentage of MB decreased from 99% to 76% as the Ci value was increased from 160 to 200 ppm. The removal amount remarkably increased from 9993 mg/g to 15,900 mg/g when the initial dye concentration increased from 100 to 160 ppm and remained stable when the concentration was increased to 200 ppm. This showed that the concentration gradient is an essential factor that drives the overcoming of the mass transfer resistances within the solid and liquid phases. The ratio of the solution connected with the α-$NiMoO_4$ surface was higher at lower MB concentrations, which triggered a rise in removal efficiency. In contrast, at higher MB dye concentrations, the decrease in the adsorption percentage was affected by the saturation of active sites on the α-$NiMoO_4$ surface [75].

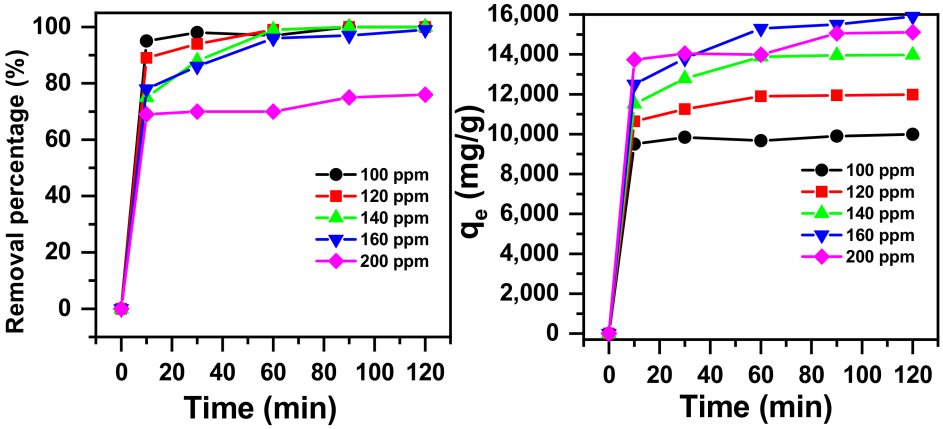

Figure 4. Impact of the initial dye concentration and contact time on the methylene blue (MB) dye removal performance of α-$NiMoO_4$ ($m_{adsorbent}$ = 0.001 g, T = 20°C, pH = 11).

2.1.5. Temperature Effect

The temperature is an essential factor that greatly affects the removal of dyes [76]. The procedure for removing the methylene blue dye was examined from 20 to 70 °C, as shown in Figure 5. The outcome of temperature experiments shows that the removal percentage increased from 70% to 100% and the removal capacity increased from 14,047 to 19,990 mg/g at an initial MB dye concentration of 200 ppm. The efficiency progression of MB removal with a rise in temperature was due to the intensity of attractive forces between removal sites and the MB, which shows an endothermic process [70]. In addition, increasing the temperature improves the removal motion of the adsorbent sites and the dye molecule motion [76].

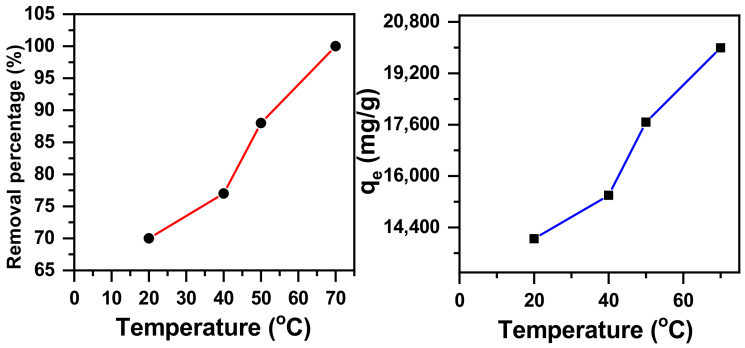

Figure 5. The effect of temperature on the dye removal capacity of $NiMoO_4$ in a 200 ppm methylene blue solution (t = 30 min, pH = 11).

Thermodynamic factors are also important factors in adsorption processes [77,78]. The probability and the mechanism of adsorption can be predicted by the thermodynamic factors [77]. The following equations are used to determine the thermodynamic parameters:

$$\Delta G^o = -RTLnK_d \quad (1)$$

$$K_d = \frac{C_a}{C_e} \quad (2)$$

$$LnK_d = \frac{\Delta S^o}{R} - \frac{H^o}{RT} \quad (3)$$

where R is the gas constant (J mol^{-1} K^{-1}), ΔG° is the free energy, K_d is the distribution constant, T is absolute temperature (K), C_a is the quantity of dye adsorbed by the adsorbent at equilibrium (mol/L), C_e is the equilibrium concentration, ΔH° is the standard enthalpy,

and ΔS° is the standard entropy. ΔS° and ΔH° values were obtained from the intercept and slope of the ln K_d versus 1/T plot (Figure 6). ΔG° values were obtained from Equation (1) and are shown in Table 1. The adsorption is favorable and spontaneous, and this is revealed by the negative value obtained for ΔG°. In fact, Gibbs free energy change (Δ*G*°) values can discern whether a process is spontaneous or not, and negative values of Δ*G*° imply a spontaneous process. The enthalpy change (Δ*H*°) provides information about the exothermic or endothermic nature of the process and differentiates between physical and chemical adsorption processes. Therefore, the positive value of ΔH° (35.12 kJ mol^{-1}) shows that methylene blue removal followed an exothermic process. In addition, the (ΔH°) value was found to be less than 40 kJ/ mol, which indicates that the adsorption of MB by nickel molybdate is physisorption [79]. The present results are similar to the results reported by Xia [80] for adsorption of congo red from aqueous solution by CTAB–hectorite and ODA–hectorite composites. The enhanced anarchy and uncertainty in the solid solution interface of methylene blue and α-$NiMoO_4$ are shown by the positive values of ΔS°. The adsorbate molecules move the adsorbed water molecules; consequently, translational energy is gained rather than lost, which indicates that this approach takes place randomly [81].

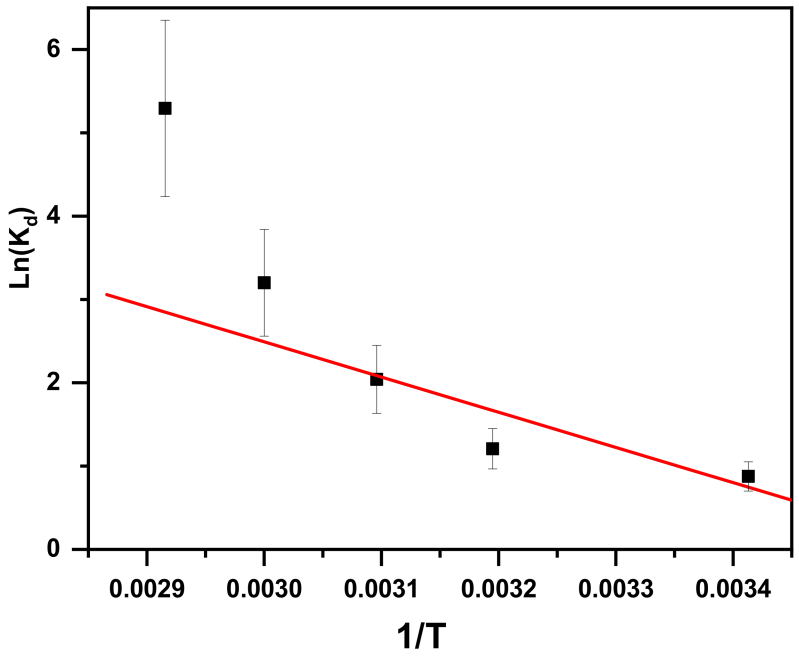

Figure 6. Van't Hoff plot presenting the impact of temperature on methylene blue dye removal utilizing α-$NiMoO_4$.

Table 1. Thermodynamic parameters for the removal of MB dye utilizing α-$NiMoO_4$.

Adsorbent	Adsorbate	Temperature (K)	K_d	ΔH° (kJ mol^{-1})	ΔS° (kJ mol^{-1} K)	ΔG° (kJ mol^{-1})				
						293K	313K	323K	333K	343K
α-$NiMoO_4$	MB	293	2.401	35.12	0.126	−2.134	−3.144	−5.480	−8.727	−14.822
		313	3.348							
		323	7.696							
		333	23.390							
		343	180.818							

2.2. Kinetic Study

Kinetic study of removal of methylene blue dye has been conducted as it provides an indication regarding the adsorption system [82].

The data found from the kinetics of removing MB dye using α-$NiMoO_4$ nanosorbent were examined by pseudo-first-order, pseudo-second-order, and intraparticle diffusion models. Equations of the studied models are shown in Table 2.

Table 2. Kinetic model equations.

Model	Equation		Parameters
Pseudo-first-order (PFD) [83]	$\mathrm{Ln}(q_e - q_t) = \mathrm{Ln}q_e + K_1 t$	(4)	K_1: the rate constant of pseudo-first-order adsorption (1/min) q_e: the removal capacity at equilibrium (mg/g) q_t: the removal capacity at time t (mg/g)
Pseudo-second-order (PSD) [83]	$\frac{t}{q_t} = \frac{1}{K_2 q_e^2} + \frac{t}{q_e}$	(5)	K_2: the pseudo-second-order rate constant ($g \cdot mg^{-1} \cdot min^{-1}$) q_e: the removal capacity at equilibrium (mg/g) q_t: the removal capacity at time t (mg/g)
Intraparticle diffusion (IPD) [77]	$q_t = K_I t^{0.5} + I$	(6)	q_t: the removal capacity (mg/g) at time t t: the contact time (min) I (mg/g) and K_I ($mg/(g \cdot min^{0.5})$): the intraparticle diffusion constants

Three model parameters, namely pseudo-first-order, pseudo-second-order, and intraparticle diffusion, are presented in Table 3 and displayed in Figure 7, Figure 8, Figure 9 respectively. Regression correlation coefficients (R^2) of the three models vary. Intraparticle diffusion is 0.934 to 0.981, pseudo-first-order ranges from 0.952 to 0.988, and pseudo-second-order is 0.999 to 1.000, varying with their concentrations used. The R^2 for pseudo-second-order is equal to or near 1, and hence this model fits very well.

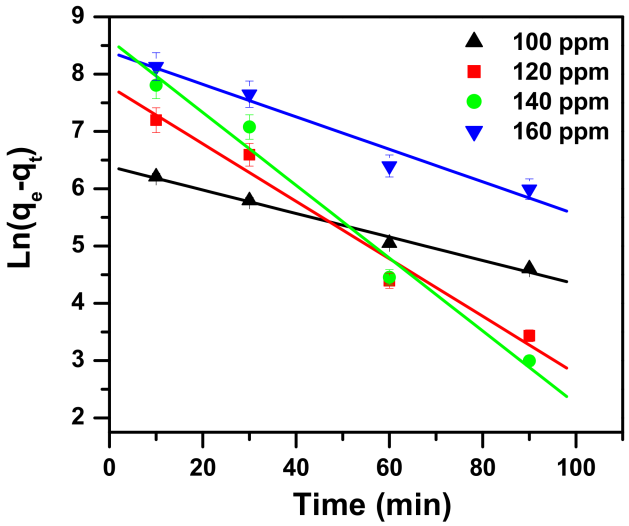

Figure 7. Pseudo-first-order model plot showing the impact of contact time and initial dye concentration on methylene blue removal utilizing α-$NiMoO_4$.

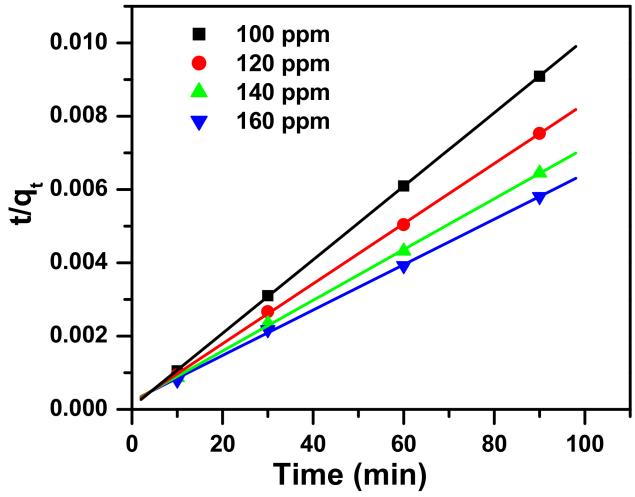

Figure 8. Pseudo-second-order model plot showing the impact of contact time and initial dye concentration on methylene blue dye removal utilizing α-$NiMoO_4$.

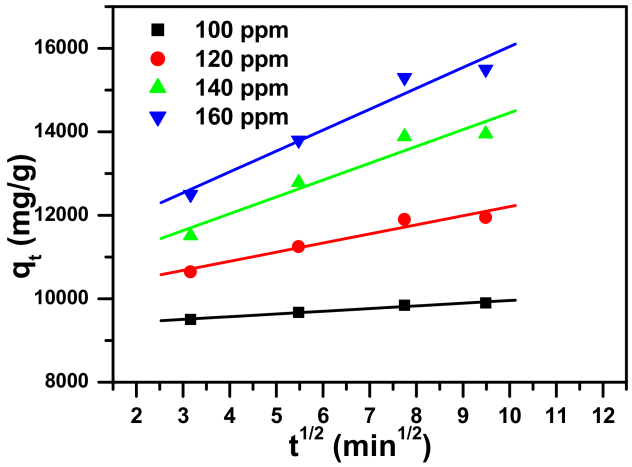

Figure 9. Intraparticle diffusion model plot showing the impact of contact time and initial dye concentration on methylene blue dye removal utilizing α-$NiMoO_4$.

Table 3. Kinetic parameters for removal of methylene blue utilizing α-$NiMoO_4$.

C_i mg/L	Pseudo-First-Order				Pseudo-Second-Order			Intraparticle Diffusion Model		
	q_{exp} (mg/g)	q_e (mg/g)	k_1 (1/min)	R_1^2	q_e (mg/g)	k_2 (g/mg min)	R_2^2	I (mg/g)	k_i (mg/g $min^{0.5}$)	R_3^2
100	10,000	584	0.020	0.988	9964	0.00015	1.000	9311	65	0.981
120	11,981	2101	0.048	0.966	12,200	0.00004	1.000	10,027	218	0.946
140	13,970	4770	0.062	0.982	14,436	0.00002	1.000	10,426	403	0.934
160	15,900	4218	0.028	0.952	16,136	0.00002	0.999	11,036	501	0.959

2.3. Adsorption Isotherms

When planning adsorption methods, adsorption isotherms, which are known to be essential, are taken into consideration due to their perfect explanation [84]. Four adsorption

models have been examined, namely Dubinin–Radushkevich, Temkin, Freundlich, and Langmuir models. Equations of the four examined models are presented in Table 4.

Table 4. Adsorption isotherm models for the removal of methylene blue dye utilizing α-$NiMoO_4$.

Model	Equation		Parameters
Freundlich [78]	$Lnq_e = Lnq_F + \frac{1}{n}LnC_e$	(7)	C_e: concentration of MB at equilibrium (ppm) n: the heterogeneity factor (g/L) q_F: the Freundlich constant ($mg^{(1-1/n)}\ L^{1/n}\ g^{-1}$) q_e: the methylene blue dye quantity adsorbed by α-NiMoO4 at equilibrium (mg/g)
Langmuir [85]	$\frac{C_e}{q_e} = \frac{1}{q_m K_L} + \frac{C_e}{q_m}$	(8)	q_e: the methylene blue dye quantity adsorbed by α-$NiMoO_4$ at equilibrium (mg/g) C_e: concentration of MB at equilibrium (ppm) q_m: the maximum quantity of methylene blue dye removed by α-$NiMoO_4$ (mg/g) K_L: Langmuir constant of adsorption (L/mg)
	$R_L = \frac{1}{1 + K_L C_i}$	(9)	C_i: the initial concentration of methylene blue K_L: the Langmuir constant R_L: values indicate that the removal of methylene blue dye could be linear (R_L = 1), irreversible (R_L = 0), favorable (0 < R_L< 1), or unfavorable (R_L > 1)
Dubinin–Radushkevich (D-R) [84]	$Lnq_e = Lnq_m - K\varepsilon^2$	(10)	K: constant for the sorption energy (mol^2/kJ^2) ε: the Polanyi potential T: the temperature (K) R: the universal gas constant (8.314 $J.mol^{-1}\ K^{-1}$) q_m: the theoretical saturation capacity C_e: the equilibrium concentration of the methylene blue dye left in the solution (ppm)
	$\varepsilon = RTLn\left(1 + \frac{1}{C_e}\right)$	(11)	
Temkin [86]	$q_e = B_T LnA_T + B_T LnC_e$	(12)	b_T: the Temkin constant related to heat of sorption (J/mol) $B_T = R_T/b_T$ R: the gas constant (8.314 J/mol K) A_T: the Temkin isotherm constant (L/g) T: the absolute temperature (K)

The models employed to match the investigational data were Freundlich, Langmuir, Temkin, and D–R isotherm. Standards of regression correlation coefficients (R^2) and the model parameters are displayed in Figure 10 and contained in Table 5. Langmuir equation demonstrated the highest value of R^2 (0.999), and D–R model revealed the lowest value of R^2 (0.782), while intermediary values were attained for Temkin and Freundlich (0.960 and 0.948, respectively). The Langmuir model fits the experimental results well; the methylene blue removal occurred on a homogeneous surface, establishing a monolayer on the α-$NiMoO_4$ adsorbent, with a high adsorption capacity of 16,863 mg/g. Methylene blue dye removal by α-$NiMoO_4$ is favorable and is revealed by the RL separation factor ranging from 0.0004 to 0.0006.

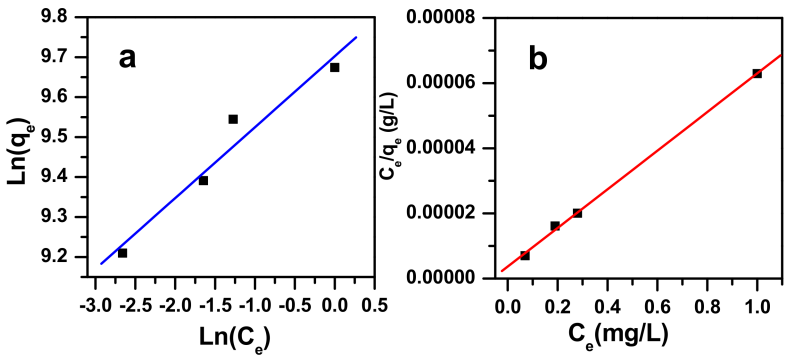

Figure 10. Freundlich (**a**) and Langmuir (**b**) isotherm model plots presenting the results of initial dye concentration and the removal of methylene blue dye utilizing α-$NiMoO_4$.

Table 5. Isotherm parameters for the removal of MB dye utilizing α-$NiMoO_4$.

Langmuir			Freundlich				Temkin			Dubinin–Radushkevich		
q_m (mg/g)	K_L (L/mg)	R^2	Range R_L	q_F($mg^{(1-1/n)}$ $L^{1/n}g^{-1}$)	1/n	R^2	A_T (L/g)	B_T	R^2	q_m (mg/g)	R^2	E (Kj/mol)
16,863	16	0.999	0.0004–0.0006	16,318	6	0.948	1220	2269	0.960	14,429	0.782	43

Table 6 presents previous reports of the maximum amount of methylene blue dye removed. When compared with many nanosorbents, Nickel-based nanosorbents NiO (Q_{max} = 10,585 mg/g) and α-$NiMoO_4$ (Q_{max} = 16,863.00 mg/g) show a considerably higher rate of adsorption for MB. The adsorption capacity of $Fe_2(MoO_4)_3$ (Q_{max} = 6173.00 mg/g) is lower than that obtained by α-$NiMoO_4$, which can be related to the difference in their specific surface area (8.03 versus 29.86 m^2/g). Thus, α-$NiMoO_4$ has the advantage of being able to be synthesized at a rather low temperature via a relatively cost-effective, very simple procedure for use in potential novel, more efficient decontamination processes aimed at the removal of methylene pollutants.

Table 6. Previous reports of the maximum amount of methylene blue dye removed (q_m).

Nanosorbent	Q_{max} (mg/g)	Reference
$ZnMoO_4$ nanoparticles	217.86	[30]
$Fe_2(MoO_4)_3$ nanoparticles	6173.00	[87]
α-MoO_3 nanoparticles	152.00	[88]
Chemically reduced graphene oxide	1519.60	[89]
Magnetic β-cyclodextrin–chitosan nanoparticles	2783.30	[90]
ZnO	7918.02–9197.70	[91]
Fe_2O_3	1124.70	[92]
CoO	5501.93	[92]
NiO	10,585.00	[92]
Nickel molybdate (α-$NiMoO_4$)	16,863.00	This work

2.4. Regeneration and Characterization of the α-$NiMoO_4$ Nanosorbent

2.4.1. Regeneration Performance

The repeatability and regeneration of nanosorbents are quite important for their practical applications. Regeneration techniques suggested in the literature include chemical extraction, thermal treatment, supercritical regeneration, microwave irradiation, bioregeneration, etc. [25,88,93–95]. The thermal regeneration, which has been applied for molybdenum oxide nanosorbent, was described in our previously published work [88]. In this investigation, the thermal treatment technique was examined for purposes of regeneration testing, as the structure of the α-$NiMoO_4$ removal agent was steady. The adsorbed MB was completely oxidized and decomposed during the calcination process.

The results showed that α-$NiMoO_4$ could be re-stimulated through thermal treatment. Figure 11 indicates the reused performance of α-$NiMoO_4$ in the removal of MB in three cycles. As a matter of fact, the data show a decrease in dye removal from 99% to 73% with a decrease in removal capacity from 15,900 to 11,608mg/g. The maximum adsorption capacity obtained after four cycles of use (11,608 mg/g) was higher than that obtained by several nanosorbents [30,87–92]. The high level of removal efficiency showed that the adsorbent regeneration by way of calcination under atmospheric air at a temperature of 400 °C was extremely efficient and indicative of outstanding recycling capability.

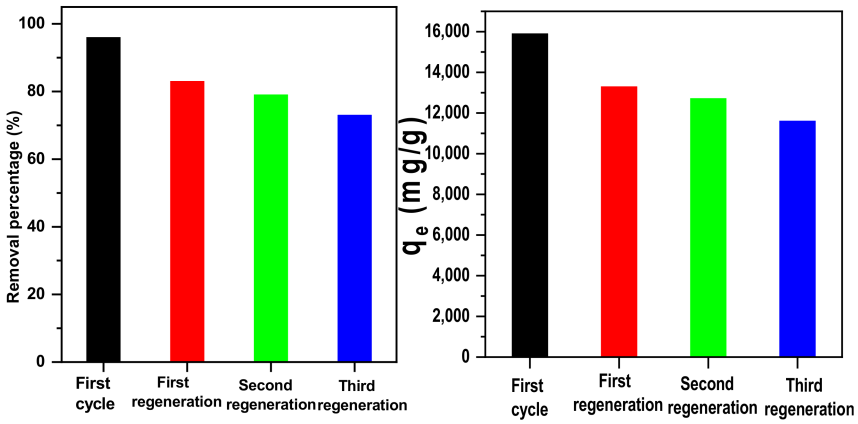

Figure 11. Recycled performance of α-$NiMoO_4$ in the removal of MB dye.

2.4.2. Fourier Transform Infrared Spectroscopy

To completely recognize the method by which α-$NiMoO_4$ nanosorbent removes MB dye, the components subjected to MB dye were examined by FT-IR spectroscopy. Figure 12 shows the FTIR spectra for the α-$NiMoO_4$ sample before and after the removal of methylene blue dye. As observed, the characteristics of flexing and stretching vibrations of the metal–oxygen bonds at 966 and 930 cm^{-1} and the broad, centered bonds at 650 cm^{-1} correspond to nickel molybdate [96]. The FTIR spectrum of the pure methylene blue displayed bands between 1700 and 1000 cm^{-1} [97]. The FTIR spectrum of $NiMoO_4$ after adsorption of methylene blue ($NiMoO_4$-MB) displayed further bands located at 1600 cm^{-1}, related to the C=C stretching of methylene blue, because of the presence of the methylene blue attached to the active sites of $NiMoO_4$ [98]. The FTIR spectrum of the regenerated $NiMoO_4$ ($NiMoO_4$-MB-Reg) after thermal treatment and the FTIR spectrum of fresh $NiMoO_4$ were alike, indicating thorough combustion of the attached methylene blue on the surface, and the resulting spectrum showed the cleanness and performance of the regenerated adsorbent.

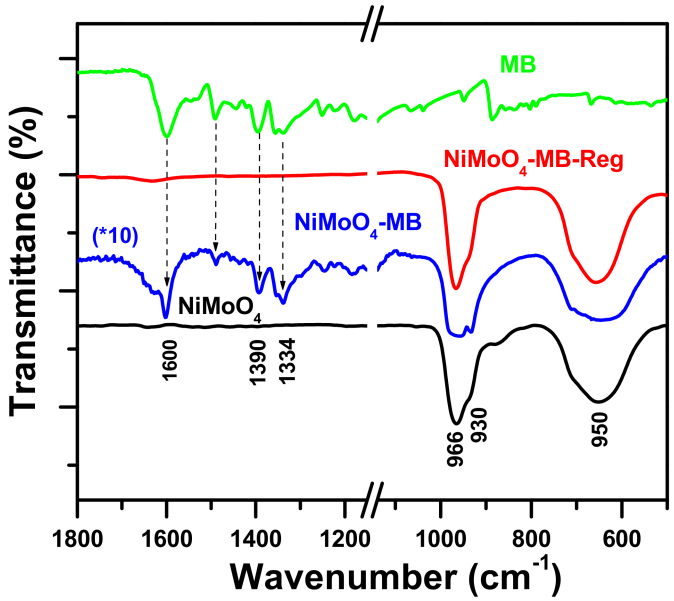

Figure 12. Fourier transform infrared spectra of $NiMoO_4$, $NiMoO_4$-MB, $NiMoO_4$-MB-Reg, and MB.

2.5. Removal Mechanism of MB

The removal of MB by α-$NiMoO_4$ nanoparticles was discovered to be due to the adsorption mechanism. Moreover, FTIR spectroscopy revealed that the removed methy-

lene blue cations were triggered by the adsorption method without any intermediate compounds produced due to the absence of MB decomposition. Additionally, by using α-$NiMoO_4$ nanoparticles, the effectiveness of MB dye removal increased with the increase in pH up to pH 11, and this may be credited to its basic media. A reasonable mechanism can be proposed (Figure 13) on the basis of these findings. Furthermore, the positive charge of the MB dye is sustained in the first step at pH 11 since the pKa is equal to 3.8 [69]. Additionally, α-$NiMoO_4$ reacts with the hydroxyl groups (OH^-) in the solution to generate the ion nickel molybdate ($NiMoO_5^{2-}$) with no intermediate compounds present [99]. Hence, the adsorption is directed by the strong electrostatic interactions between the negatively charged surface of nickel molybdate ($NiMoO_5^{2-}$) and the positive charge of methylene blue cations [88].

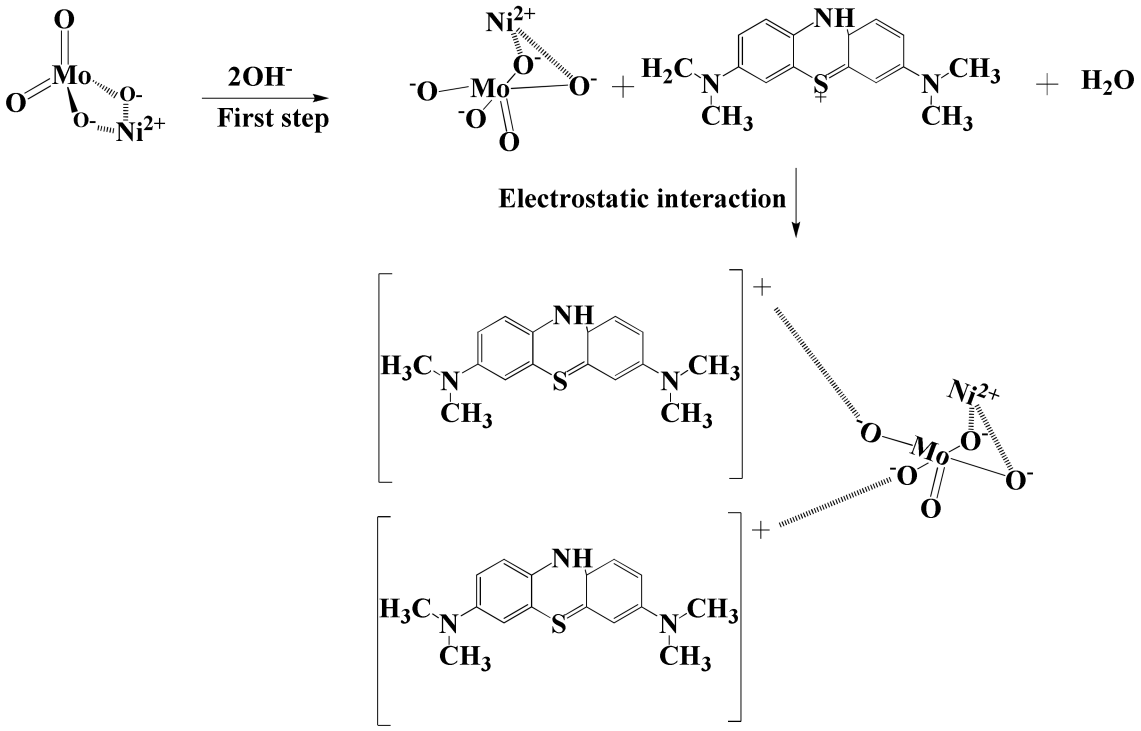

Figure 13. Schematic mechanism of the methylene blue dye removal by α-$NiMoO_4$ nanosorbent.

It is important to adhere to the progression of the α-$NiMoO_4$ morphology at different phases of the adsorption study. The SEM micrograph in Figure 14A gives an idea about how the particles form aggregates, showing a good porosity that can allow the improved adsorption of the dye. Nevertheless, the micrographs in Figure 14B,D,F show much less porous powder after the adsorption experiments; the methylene blue molecules filled the pores present in the starting samples. Figure 14C,E,G shows that the morphology of the sample did not change after the regeneration or the first and second reuses. In all cases, the particles were less agglomerated, displaying exceptionally porous powder. The morphology of α-$NiMoO_4$ was not significantly altered, even after the second and third reuses (Figure 14E,G).

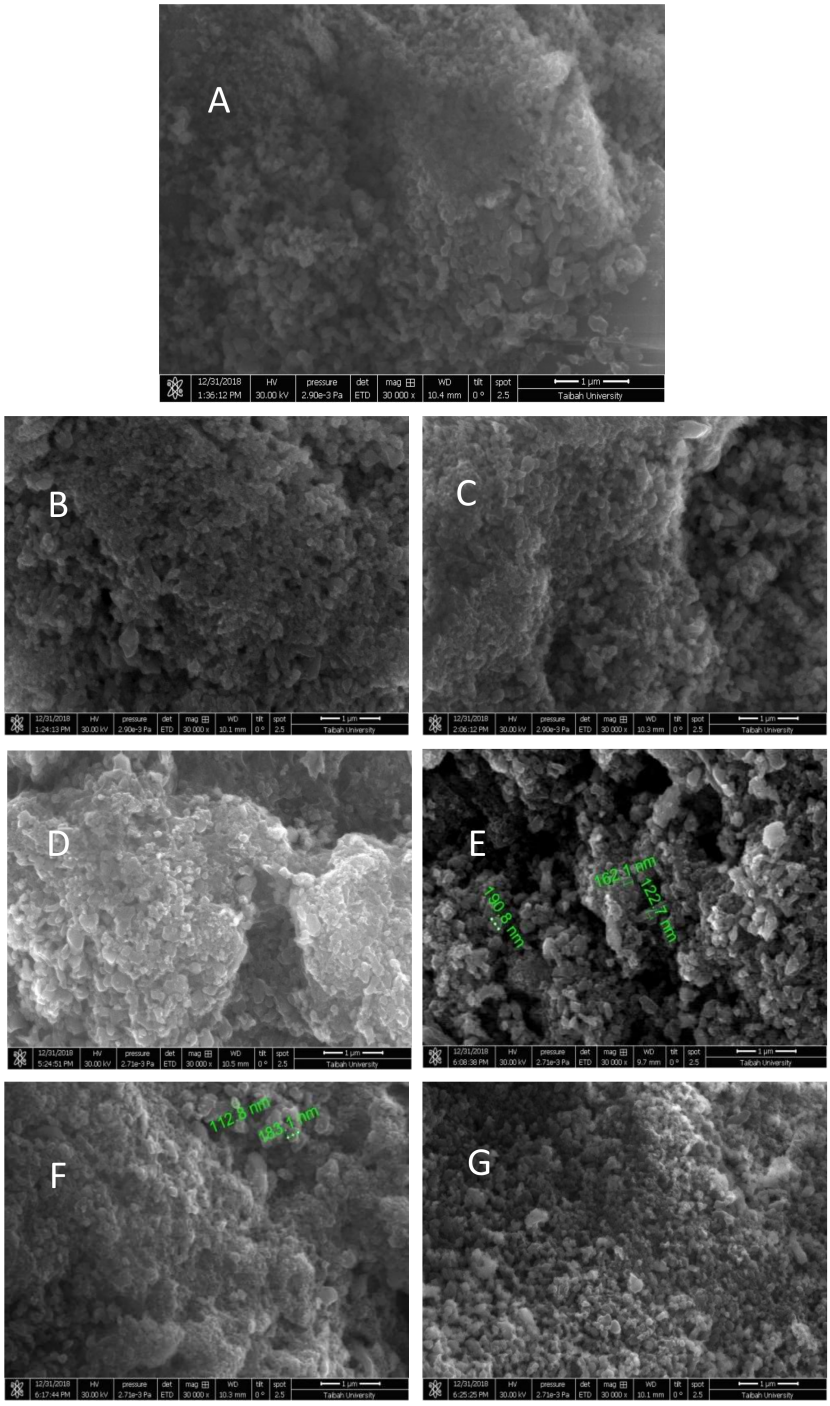

Figure 14. SEM micrographs: (**A**) the starting material, pure nickel molybdate (α-$NiMoO_4$); (**B**) the material after the MB dye had been removed; (**C**) the regenerated α-$NiMoO_4$; (**D**) the material after the second regeneration and/or removal cycle of the methylene blue dye; (**E**) the morphology of α-$NiMoO_4$ after the second regeneration process; (**F**) the material after the third regeneration/removal cycle of methylene blue dye; (**G**) the morphology of α-$NiMoO_4$ after the third regeneration.

3. Materials and Methods

3.1. Nickel Molybdate Nanosorbent Preparation

All synthetic compounds aside from the methylene blue (provided by Panreac, Barcelona, Spain) were purchased from Sigma-Aldrich (St. Louis, MO, USA) and utilized as received with no alterations.

Nickel molybdate ($NiMoO_4$) was formed by thermal breakdown of a nickel molybdenum complex obtained from the reaction of oxalic acid dihydrate $H_2C_2O_4{\cdot}2H_2O$, nickel nitrate $Ni(NO_3)_2{\cdot}6H_2O$, and ammonium molybdate $(NH_4)_6Mo_7O_{24}{\cdot}4H_2O$ in its solid form, as defined previously in the literature [32]. Nickel nitrate, oxalic acid dihydrate, and ammonium molybdate were blended jointly together in a molar proportion of 1/10/0.143. The mixture was powdered homogeneously and placed on a hot plate at a temperature of 160 °C for heating. The obtained nickel molybdenum complex was then decomposed under the control with static air at 500 °C for 2 h inside a cylindrical furnace, which was open at the two ends.

3.2. Adsorption Experiments

Experimental adsorption batches were set up for the removal of the MB dye [75]. The elimination of MB dye by $NiMoO_4$ was undertaken by the constant stirring of a precise quantity of adsorbent into a 100 mL MB dye solution with known concentrations and varied temperatures (such as T = 20, 50, and 70 °C) with various contact times (such as 10, 30, 60, 90, and 120 min). Toward the end of prearranged time intervals, before examination with a UV-Visible spectrometer, 0.22 µm syringe filters (Whatman) were used for filtration. Using 0.01 N NaOH or 0.01 N HCl, the pH of the methylene blue solution was easily adjusted. The removed quantity and percentage (%) of methylene blue dye at its equilibrium q_e (mg/g) were calculated by the following equations:

$$\text{Removal } \% = \frac{C_0 - C_e}{C_0} \times 100 \tag{13}$$

$$q_e = \frac{(C_0 - C_e)}{M} \times V \tag{14}$$

where M stands for the mass of α-$NiMoO_4$ (g) added; V is the quantity of solution used (L); and C_e and C_0 are equilibrium and initial concentrations of MB (ppm), respectively. The results were tested three consecutive times, and the percentage uncertainty was found to be around 3%.

3.3. Adsorbent Regeneration Method

A solution of 160 ppm was used for regeneration experiments, and the removal equilibrium period was extended by 1 h. The fresh α-$NiMoO_4$ used was filtered and dried under a constant temperature of 100 °C and then calcined at 400 °C for 1 h under atmospheric air. The calcined α-$NiMoO_4$ was examined to assess the recycling objectives under conditions similar to those for the freshly used α-$NiMoO_4$. Once the first recycling test worked well, the restoration process was replicated for three consecutive cycles under consistent conditions.

3.4. pH Point of Zero Charge (pH_{pzc}) Measure

The pH point of zero charge (pHpzc) of the material was measured by the electrochemical method reported by Altenor et al. [100]. First, 50 mL of a 0.01 M NaCl solution was placed in a 100 mL beaker. Then, the pH was adjusted to successive initial values between 2 and 12 by using either NaOH or HCl (0.1 M), and 0.001 g of nickel molybdate was added to the solutions. After a contact time of 24 h, the final pH was measured and plotted against the initial pH.

3.5. Characterization

Analysis of XRD patterns (X-ray diffractometer 6000, Shimadzu, Tokyo, Japan, installed with $\lambda_{Cu\text{-}K\alpha}$ = 1.5406 Å and Ni filter) was conducted to characterize the phase composition of the synthesized α-$NiMoO_4$ nanosorbent, as presented in Figure 15.

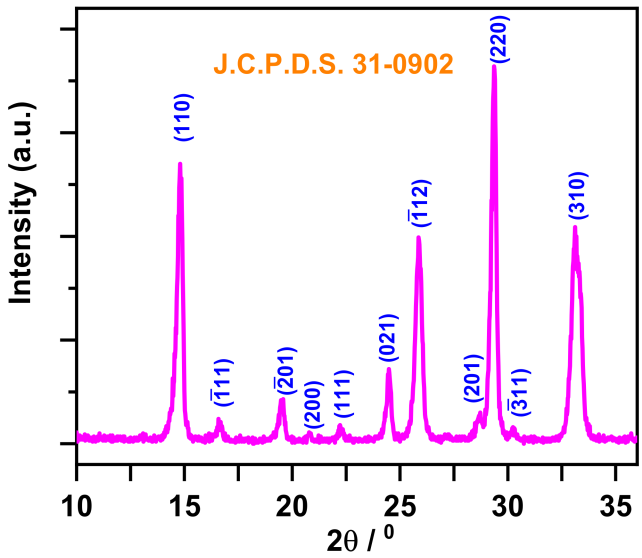

Figure 15. X-ray diffraction pattern of the synthesized $NiMoO_4$ nanoparticle powder. The Joint Committee on Powder Diffraction Standards (J.C.P.D.S) index file number is 31-0902.

The specific surface area characterization was completed by using nitrogen isotherm adsorption in the same way as stated in our previous research work [32]. The recorded specific surface area was 29.86 m^2/g.

FTIR spectroscopy in the range of 400 to 4000 cm^{-1} (IR Affinity-1S Shimadzu apparatus, Tokyo, Japan) using KBr pellets confirmed the existence of methylene blue dye on α-$NiMoO_4$ nanoparticles following the experimental adsorption and regeneration studies.

SEM analysis (Quanta Feg 250, Thermo Fisher Scientific, Hillsboro, OR, USA) was conducted. UV-Visible spectrophotometer (Thermo Scientific Genesys 10S, Madison, WI, USA) was used to determine the concentration at equilibrium.

4. Conclusions

α-$NiMoO_4$ nanosorbent was synthesized and investigated as a material for the removal of MB dye from aqueous solutions. Removal of MB was extremely reliant on the pH, and this resulted in the achievement of 99% removal efficiency for initial dye concentrations between 100 and 160 ppm at pH 11. The kinetic findings suggested that the removal of methylene blue followed the pseudo-second-order model, and the equilibrium adsorption results were best fitted with the Langmuir isotherm model. The highest removal amount achieved was 16,863 mg/g, as determined by the Langmuir model. Calcination at 400 °C was effectively sufficient to regenerate the adsorbent for further reuse. Even after three cycles of reusing the adsorbent, the MB removal efficiency of $NiMoO_4$ was still high. The data proved that α-$NiMoO_4$ could be an effective nanosorbent offering outstanding performance in removing MB dye even after being recycled.

Author Contributions: Conceptualization, S.R., H.O.H., and A.M.; Methodology, S.R., H.O.H., and A.M.; Validation, S.R., H.O.H., F.K., M.A., E.A., F.A.W. and A.M.; Formal Analysis, H.O.H., S.R., A.M., M.A., and F.K.; Investigation, S.R., H.O.H., A.M., F.K., M.A. and E.A.; Resources, H.O.H., M.A., F.K., F.A.W., E.A. and S.R.; Data Curation, H.O.H., S.R., A.M., M.A., F.K. and E.A.; Writing-Original Draft Preparation, S.R., H.O.H. and A.M.; Writing-Review & Editing, F.K., M.A, S.R., A.M. and H.O.H.; Visualization, S.R., H.O.H., F.K., A.M., M.A., E.A. and F.A.W.; Supervision, S.R., and H.O.H.; Project Administration, S.R. and H.O.H.; Funding Acquisition, E.A., F.A.W. and M.A. All authors have read and agreed to the published version of the manuscript.

Funding: This research received no external funding.

Data Availability Statement: The data that support the findings of this study are available from the corresponding author upon reasonable request.

Conflicts of Interest: The authors declare no conflict of interest.

Sample Availability: Samples of the compounds NiMoO4 are available from the corresponding author.

References

1. Khin, M.M.; Nair, A.S.; Babu, V.J.; Murugana, R.; Ramakrishna, S. A review onnanomaterials for environmental remediation. *Energy Environ. Sci.* **2012**, *5*, 8075–8109. [CrossRef]
2. Colmenares, J.C.; Luque, R. Heterogeneous photocatalytic nanomaterials: Prospects and challenges in selective transformations of biomass-derived compounds. *Chem. Soc. Rev.* **2014**, *43*, 765–778. [CrossRef]
3. Madrakian, T.; Afkhami, A.; Ahmadi, M.; Bagheri, H. Removal of some cationic dyes from aqueous solutions using magnetic modified multi-walled carbon nanotubes. *J. Hazard. Mater.* **2011**, *196*, 109–114. [CrossRef]
4. Yang, N.; Zhu, S.; Zhang, D.; Xu, S. Synthesis and properties of magnetic Fe_3O_4-activated carbon nanocomposite particles for dye removal. *Mater. Lett.* **2008**, *62*, 645–647. [CrossRef]
5. Sucharita, A. Textile Dyes: Its Impact on Environment and its Treatment. *J. Bioremediat. Biodegrad.* **2014**, *5*, 1.
6. Solis, M.; Solis, A.; Perez, H.I.; Manjarrez, N.; Flores, M. Microbial decolouration of azo dyes: A review. *Process Biochem.* **2012**, *47*, 1723–1748. [CrossRef]
7. Elemen, S.; Kumbasar, E.P.A.; Yapar, S. Modeling the adsorption of textile dye on organoclay using an artificial neural network. *Dye. Pigment.* **2012**, *95*, 102–111. [CrossRef]
8. Greluk, M.; Hubicki, Z. Effect of basicity of anion exchangers and number and positions of sulfonic groups of acid dyes on dyes adsorption on macroporous anion exchangers with styrenic polymer matrix. *Chem. Eng. J.* **2013**, *215–216*, 731–739. [CrossRef]
9. Turgay, O.; Ersoz, G.; Atalay, S.; Forss, J.; Welander, U. The treatment of azo dyes found in textile industry wastewater by anaerobic biological method and chemical oxidation. *Sep. Purif. Technol.* **2011**, *79*, 26–33. [CrossRef]
10. Verma, A.K.; Dash, R.R.; Bhunia, P. A review on chemical coagulation/flocculation technologies for removal of colour from textile wastewaters. *J. Environ. Manag.* **2012**, *93*, 154–168. [CrossRef]
11. Kanagaraj, J.; Senthilvelan, T.; Panda, R.C. Degradation of azo dyes by laccase: Biological method to reduce pollution load in dye wastewater. *Clean Technol. Environ. Policy* **2015**, *17*, 1443–1456. [CrossRef]
12. Cornelia, P.; Oana, P.; Robert, I.; Simona, G.M. Effective removal of methylene blue from aqueous solution using a new magnetic iron oxide nanosorbent prepared by combustion synthesis. *Clean Technol. Environ. Policy* **2016**, *18*, 705–715.
13. Vanhulle, S.; Trovaslet, M.; Enaud, E.; Lucas, M.; Taghavi, S.; van der Lelie, D.; van Aken, B.; Foret, M.; Onderwater, R.C.A.; Wesenberg, D.; et al. Decolorization, cytotoxicity and genotoxicity reduction during a combined ozonation/fungal treatment of dye-contaminated wastewater. *Environ. Sci. Technol.* **2008**, *42*, 584–589. [CrossRef]
14. Forgacs, E.; Cserhati, T.; Oros, G. Removal of synthetic dyes from wastewaters: A review. *Environ. Int.* **2004**, *30*, 953–971. [CrossRef]
15. Filice, S.; Angelol, D.D.; Libertinol, S.; Kosma, V.; Nicotera, I.; Privitera, V.; Scalese, S. Graphene oxide and titania hybrid Nation membranes for efficient removal of methyl orange dye from water. *Carbon* **2015**, *82*, 489–499. [CrossRef]
16. Kang, S.; Zhao, Y.; Wang, W.; Zhang, T.; Chen, T.; Yi, H.; Rao, F.; Song, S. Removal of methylene blue from water with montmorillonite nanosheets/chitosan hydrogels as adsorbent. *Appl. Surf. Sci.* **2018**, *448*, 203–211. [CrossRef]
17. Miyah, Y.; Lahrichi, A.; Idrissi, M.; Khalil, A.; Zerrouq, F. Adsorption of methylene blue dye from aqueous solutions onto walnut shells powder: Equilibrium and kinetic studies. *Surf. Interface* **2018**, *11*, 74–81. [CrossRef]
18. Ozdemir, U.; Ozbay, I.; Ozbay, B.; Veli, S. Application of economical models for dye removal from aqueous solutions: Cash flow, cost–benefit and alternative selection methods. *Clean Technol. Environ. Policy* **2014**, *16*, 423–429. [CrossRef]
19. Chen, Y.H. Synthesis, characterization and dye adsorption of ilmenite nanoparticles. *J. Non-Cryst. Solids* **2011**, *357*, 136–139. [CrossRef]
20. Sadhukhan, B.; Mondal, N.K.; Chattoraj, S. Biosorptive removal of cationic dye from aqueous system: A response surface methodological approach. *Clean Technol. Environ. Policy* **2014**, *16*, 1015–1025. [CrossRef]
21. George, Z.; Kyzas, J.F.; Kostas, A.M. The Change from Past to Future for Adsorbent Materials in Treatment of Dyeing Wastewaters. *Materials* **2013**, *6*, 5131–5158.
22. Mouni, L.; Belkhiri, L.; Bollinger, J.C.; Bouzaza, A.; Assadi, A.; Tirri, A.; Dahmoune, F.; Madani, K.; Remini, H. Removal of methylene blue from aqueous solutions by adsorption on Kaolin: Kinetic and equilibrium studies. *Appl. Clay Sci.* **2018**, *153*, 38–45. [CrossRef]
23. Bentahar, S.; Dbik, A.; El Khomri, M.; El Messaoudi, N.; Lacherai, A. Removal of a cationic dye from aqueous solution by natural clay. *Groundw. Sustain. Dev.* **2018**, *6*, 255–262. [CrossRef]
24. Low, S.K.; Tan, M.C. Dye adsorption characteristic of ultrasound pre-treated pomelo peel. *J. Environ. Chem. Eng.* **2018**, *6*, 3502–3509. [CrossRef]
25. Rakass, S.; Mohmoud, A.; Oudghiri-Hassani, H.; Abboudi, M.; Kooli, F.; Al Wadaani, F. Modified Nigella Sativa Seeds as a Novel Efficient Natural Adsorbent for Removal of Methylene Blue Dye. *Molecules* **2018**, *23*, 1950. [CrossRef] [PubMed]
26. Ghaedi, M.; Tavallali, H.; Sharifi, M.; NasiriKokhdan, S.; Asghari, A. Preparation of low cost activated carbon from Myrtuscommunis and pomegranate and their efficient application for removal of Congo red from aqueous solution. *Spectrochim. Acta Part A* **2012**, *86*, 107–114. [CrossRef] [PubMed]

27. Taghizadeh, F.; Ghaedi, M.; Kamali, K.; Sharifpour, E.; Sahraie, R.; Purkait, M.K. Comparison of nickel and/or zinc selenide nanoparticle loaded on activated carbon as efficient adsorbents for kinetic and equilibrium study of removal of Arsenazo (III) dye. *Powder Technol.* **2013**, *245*, 217–226. [CrossRef]
28. Singh, K.P.; Gupta, S.; Singh, A.K.; Sinha, S. Optimizing adsorption of crystal violet dye from water by magnetic nanocomposite using response surface modeling approach. *J. Hazard. Mater.* **2011**, *186*, 1462–1473. [CrossRef]
29. Yufei, Z.; Laiquan, L.; Haiquan, S.; Wei, H.; Xiaochen, D. Binary metal oxide: Advanced energy storage materials in supercapacitors. *J. Mater. Chem. A* **2015**, *3*, 43–59.
30. Oudghiri-Hassani, H.; Rakass, S.; Abboudi, M.; Mohmoud, A.; Al Wadaani, F. Preparation and Characterization of α-Zinc Molybdate Catalyst: Efficient Sorbent for Methylene Blue and Reduction of 3-Nitrophenol. *Molecules* **2018**, *23*, 1462. [CrossRef]
31. Oudghiri-Hassani, H. Synthesis, characterization and catalytic performance of iron molybdate Fe_2 $(MoO_4)_3$ nanoparticles. *Catal. Commun.* **2015**, *60*, 19–22. [CrossRef]
32. Oudghiri-Hassani, H.; Al Wadaani, F.T. Preparation, Characterization and Catalytic Activity of Nickel Molybdate ($NiMoO_4$) Nanoparticles. *Molecules* **2018**, *23*, 273. [CrossRef]
33. Al-Wadaani, F.; Omer, A.; Abboudi, M.; Oudghiri-Hassani, H.; Rakass, S.; Messali, M.; Benaissa, M. High Catalytic Efficiency of Nanostructured β-$CoMoO_4$ in the Reduction of the Ortho-, Meta- and Para-Nitrophenol Isomers. *Molecules* **2018**, *23*, 364. [CrossRef] [PubMed]
34. Madeley, R.A.; Wanke, S. Variation of the dispersion of active phases in commercial nickel—molybdenum/γ-alumina hydrotreating catalysts during oxidative regeneration. *Appl. Catal.* **1988**, *39*, 295–314. [CrossRef]
35. Gates, B.C.; Katzer, J.R.; Schuit, G.C.A. *Chemistry of Catalytic Processes*; McGraw-Hill: New York, NY, USA, 1979; p. 390.
36. Kaddouri, A.; Anouchinsky, R.; Mazzocchia, C.; Madeira, L.M.; Portela, M.F. Oxidative dehydrogenation of ethane on the α and β phases of $NiMoO_4$. *Catal. Today* **1998**, *40*, 201–206. [CrossRef]
37. Pillay, B.; Mathebula, M.R.; Friedrich, H.B. The oxidative dehydrogenation of *n*-hexane over Ni–Mo–O catalysts. *Appl. Catal. A* **2009**, *361*, 57–64. [CrossRef]
38. Rodriguez, J.A.; Chaturvedi, S.; Hanson, J.C.; Brito, J.L. Reaction of H_2 and H_2S with $CoMoO_4$ and $NiMoO_4$: TPR, XANES, Time-Resolved XRD, and Molecular-Orbital Studies. *J. Phys. Chem.* **1999**, *103*, 770–781. [CrossRef]
39. Sundaram, R.; Nagaraja, K.S. Solid state electrical conductivity and humidity sensing studies on metal molybdate–molybdenum trioxide composites (M = Ni^{2+}, Cu^{2+} and Pb^{2+}). *Sens. Actuators B Chem.* **2004**, *101*, 353–360. [CrossRef]
40. Mi, Y.; Huang, Z.; Hu, F.; Jiang, J.; Li, Y. Controlled synthesis and growth mechanism of alpha nickel molybatemicrohombohedron. *Mater. Lett.* **2010**, *64*, 695–697. [CrossRef]
41. Brito, J.L.; Barbosa, A.L.; Albornoz, A.; Severino, F. Nickel molybdate as precursor of HDS catalysts: Effect of phase composition. *Catal. Lett.* **1994**, *26*, 329–337. [CrossRef]
42. Ryu, J.H.; Koo, S.M.; Yoon, J.W.; Lim, C.S.; Shim, K.B. Synthesis of nanocrystalline $MMoO_4$ (M = Ni, Zn) phosphors via a citrate complex route assisted by microwave irradiation and their photoluminescence. *Mater. Lett.* **2006**, *60*, 1702–1705. [CrossRef]
43. Chen, Y.; Meng, F.; Ma, C.; Yang, Z.; Zhu, C.; Ouyang, Q.; Gao, P.; Li, J.; Sun, C. In situ diffusion growth of Fe_2 $(MoO_4)_3$ nanocrystalson the surface of α-MoO_3 nanorods with significantly enhanced ethanol sensing properties. *J. Mater. Chem.* **2012**, *22*, 12900–12906. [CrossRef]
44. Senthilkumar, B.; VijayaSankar, K.; Selvan, R.K.; Danielle, M.; Manickam, M. Nano α-$NiMoO_4$ as a new electrode for electrochemical supercapacitors. *RSC Adv.* **2013**, *3*, 352–357. [CrossRef]
45. Liu, M.; Kong, L.; Lu, C.; Li, X.; Luo, Y.; Kang, L. Waste paper based activated carbon monolith as electrode materials for high performance electric double-layer capacitors. *RSC Adv.* **2012**, *2*, 1890–1896. [CrossRef]
46. Liu, P.; Deng, Y.; Zhang, Q.; Hu, Z.; Xu, Z.; Liu, Y.; Yao, M.; Ai, Z. Facile synthesis and characterization of high-performance $NiMoO_4 \cdot xH_2O$ nanorods electrode material for supercapacitors. *Ionics* **2015**, *21*, 2797–2804. [CrossRef]
47. Cherian, C.T.; Reddy, M.V.; Haur, S.C.; Chowdari, B.V.R. Interconnected Network of $CoMoO_4$ Submicrometer Particles As High Capacity Anode Material for Lithium Ion Batteries. *ACS Appl. Mater. Interfaces* **2013**, *5*, 918–923. [CrossRef] [PubMed]
48. Ding, Y.; Yu, S.H.; Liu, C.; Zang, Z.A. 3D Architectures of Iron Molybdate: Phase Selective Synthesis, Growth Mechanism, and Magnetic Properties. *Chem. Eur. J.* **2007**, *13*, 746–753. [CrossRef]
49. Saberyan, K.; Soofivand, F.; Kianpour, G.; Salavati-Niasari, M.; Bagheri, S. Synthesis and characterization of $NiMoO_4$ via ultrasonic route by a novel precursor. *J. Mater. Sci. Mater. Electron.* **2016**, *27*, 3765–3772. [CrossRef]
50. Kianpour, G.; Salavati-Niasari, M.; Emadi, H. Sonochemical synthesis and characterization of $NiMoO_4$nanorods. *Ultrason. Sonochem.* **2013**, *20*, 418–424. [CrossRef]
51. Cai, D.; Wang, D.; Liu, B.; Wang, Y.; Liu, Y.; Wang, L.; Li, H.; Li, H.Q.; Wang, T. Comparison of the Electrochemical Performance of $NiMoO_4$ Nanorods and Hierarchical Nanospheres for Supercapacitor Applications. *ACS Appl. Mater. Interfaces* **2013**, *5*, 12905–12910. [CrossRef]
52. Ray, S.K.; Dipesh, D.; Yuwaraj, K.K.; Soo, W.L. Cu-α-$NiMoO_4$photocatalyst for degradation of Methylene blue with pathways and antibacterial performance. *J. Photochem. Photobiol. A* **2017**, *348*, 18–32. [CrossRef]
53. Kaddouri, A.; Tempesti, E.; Mazzocchia, C. Comparative study of β-nickel molybdate phase obtained by conventional precipitation and the sol-gel method. *Mater. Res. Bull.* **2004**, *39*, 695–706. [CrossRef]
54. Mosleh, M. Facile approach to synthesize nanocristalline $NiMoO_4$ in the presence of amino acids as capping agent. *J. Mater. Sci. Mater. Electron.* **2017**, *28*, 6788–6793. [CrossRef]

55. Klissurski, D.; Mancheva, M.; Iordanova, R.; Kunev, B. Mechanochemical Synthesis of Nanocrystalline Nickel Molybdates. *J. Alloys Compd.* **2006**, *422*, 53–57. [CrossRef]
56. Maione, A.; Devilers, M. Solid Solutions of Ni and Co Molybdates in Silica-Dispersed and Bulk Catalysts Prepared by Sol-Gel and Citrate Methods. *J. Solid State Chem.* **2004**, *177*, 2339–2349. [CrossRef]
57. Saravanakumar, B.; Ramachandran, S.P.; Ravi, G.; Ganesh, V.; Sakunthala, A.; Yuvakkumar, R. Morphology dependent electrochemical capacitor performance of $NiMoO_4$ nanoparticles. *Mater. Lett.* **2017**, *209*, 1–4. [CrossRef]
58. Azadeh, T.; Raheleh, P.; Mina, I.; Samaneh, E.; Mohammad, S. A simplified microwave-assisted synthesis of $NiMoO_4$ nanoparticles by using organic driving agent and study of photocatalytic activity. In Proceedings of the 18th International Electronic Conference on Synthetic Organic Chemistry Session Microwave Assisted Synthesis, 1–30 November 2014.
59. Edrissi, M.; Samadanian-Isfahani, S.; Soleymani, M. Preparation of cobalt molybdate nanoparticles; Taguchi optimization and photocatalytic oxidation of Reactive Black 8 dye. *Powder Technol.* **2013**, *249*, 378–385. [CrossRef]
60. Ghoreishiana, S.M.; Raju, G.S.R.; Pavitra, E.; Kwak, C.H.; Han, Y.K.; Huh, Y.S. Controlled synthesis of hierarchical α-nickel molybdate with enhanced solar-light-responsive photocatalytic activity: A comprehensive study on the kinetics and effect of operational factors. *Ceram. Int.* **2019**, *45*, 12041–12052. [CrossRef]
61. Ferreira, E.A.C.; Andrade Neto, N.F.; Bomio, M.R.D.; Motta, F.V. Influence of solution pH on forming silver molybdates obtained by sonochemical method and its application for methylene blue degradation. *Ceram. Int.* **2019**, *45*, 11448–11456. [CrossRef]
62. Rashad, M.M.; Ibrahim, A.A.; Rayan, D.A.; Sanad, M.M.S.; Helmy, I.M. Photo-Fenton-like degradation of Rhodamine B dye from waste water using iron molybdate catalyst under visible light irradiation. *Environ. Nanotechnol. Monit. Manag.* **2017**, *8*, 175–186. [CrossRef]
63. Oudghiri-Hassani, H. Synthesis, Characterization and Application of Chromium molybdate for Oxidation of Methylene Blue Dye. *J. Mater. Environ. Sci.* **2018**, *9*, 1051–1057.
64. Kianpour, G.; Soofivand, F.; Badiei, M.; Salavati-Niasari, M.; Hamadanian, M. Facile synthesis and characterization of nickel molybdatenanorods as an effective photocatalyst by co-precipitation method. *J. Mater. Sci. Mater. Electron.* **2016**, *27*, 10244–10251. [CrossRef]
65. Dhanasekar, M.; Ratha, S.; Rout, C.S.; Bhat, S.V. Efficient sono-photocatalytic degradation of methylene blue using nickel molybdate nanosheets under diffused sunlight. *J. Environ. Chem. Eng.* **2017**, *5*, 2997–3004. [CrossRef]
66. Abia, A.A.; Asuquo, E.D. Lead (II) and nickel (II) adsorption kinetics from aqueous metal solutions using chemically modified and unmodified agricultural adsorbents. *Afr. J. Biotechnol.* **2006**, *5*, 1475–1482.
67. Yogesh Kumar, K.; Archana, S.; Vinuth Raj, T.N.; Prasana, B.P.; Raghu, M.S.; Muralidhara, H.B. Superb Adsorption Capacity of Hydrothermally Synthesized Copper oxide and Nickel oxide nanoflakes towards Anionic and Cationic dyes. *J. Sci. Adv. Mater. Dev.* **2017**, *2*, 183–191. [CrossRef]
68. Alver, E.; Metin, A.U. Anionic dye removal from aqueous solutions using modified zeolite: Adsorption kinetics and isotherm studies. *Chem. Eng. J.* **2012**, *200–202*, 59–67. [CrossRef]
69. Jihyun, R.K.; Santiano, B.; Kim, H.; Kan, E. Heterogeneous Oxidation of Methylene Blue with Surface-Modified Iron-Amended Activated Carbon. *Am. J. Anal. Chem.* **2013**, *4*, 115–122.
70. Kooli, F.; Liu, Y.; Abboudi, M.; Oudghiri Hassani, H.; Rakass, S.; Ibrahim, S.M.; Al-Wadaani, F. Waste bricks applied as removal agent of Basic Blue 41 from aqueous solution: Base treatment and their regeneration efficiency. *Appl. Sci.* **2019**, *9*, 1237. [CrossRef]
71. Santhi, T.; Manonmani, S. Adsorption of methylene blue from aqueous solution onto a waste aquacultural shell powders (prawn waste). *Sustain. Environ. Res.* **2012**, *22*, 45–51.
72. Kooli, F.; Liu, Y.; Hbaieb, K.; Ching, O.Y.; Al-Faze, R. Characterization of organo-kenyaites: Thermal stability and their effects on eosin removal characteristics. *Clay Miner.* **2018**, *53*, 91–104. [CrossRef]
73. Alzaydien, A.S. Adsorption Behavior of Methyl Orange onto Wheat Bran: Role of Surface and pH. *Orient. J. Chem.* **2015**, *31*, 643–651. [CrossRef]
74. Garg, V.K.; Gupta, R.; Yadav, A.B.; Kumar, R. Dye removal from aqueous solution by adsorption on treated sawdust. *Bioresour. Technol.* **2003**, *89*, 121–124. [CrossRef]
75. Mahmoud, D.K.; Salleh, M.A.M.; Karim, W.A.W.A.; Idris, A.; Abidin, Z.Z. Batch adsorption of basic dye using acid treated kenaf fibre char: Equilibrium, kinetic and thermodynamic studies. *Chem. Eng. J.* **2012**, *181–182*, 449–457. [CrossRef]
76. Wawrzkiewicz, M.; Hubicki, Z. Removal of tartrazine from aqueous solutions by strongly basic polystyrene anion exchange resins. *J. Hazard. Mater.* **2009**, *164*, 502–509. [CrossRef] [PubMed]
77. Furusawa, T.; Smith, J.M. Intraparticle mass transport in slurries by dynamic adsorption studies. *AIChE J.* **1974**, *20*, 88–93. [CrossRef]
78. Foo, K.Y.; Hameed, B.H. Insights into the modeling of adsorption isotherm systems. *Chem. Eng. J.* **2010**, *156*, 2–10. [CrossRef]
79. Ma, J.; Jia, Y.; Jing, Y.; Yao, Y.; Sun, J. Kinetics and thermodynamics of methylene blue adsorption by cobalt-hectorite composite. *Dye. Pigment.* **2012**, *93*, 1441–1446. [CrossRef]
80. Chenglong, X.; Yan, J.; Yongzhong, J.; Duyuan, Y.; Jun, M.; Xiaojie, Y. Adsorption properties of congo red from aqueous solution on modified hectorite: Kinetic and thermodynamic studies. *Desalination* **2011**, *265*, 81–87.
81. Vadivelan, V.; Kumar, K.V. Equilibrium, kinetics, mechanism and process design for the sorption of methylene blue onto rice husk. *J. Colloid Interface Sci.* **2005**, *286*, 90–100. [CrossRef]

82. Febrianto, J.; Kosasih, A.N.; Sunarso, J.; Ju, Y.; Indraswati, N.; Ismadji, S. Equilibrium and kinetic studies in adsorption of heavy metals using biosorbent: A summary of recent studies. *J. Hazard. Mater.* **2009**, *162*, 616–645. [CrossRef] [PubMed]
83. Ho, Y.S.; McKay, G. Pseudo-second order model for sorption processes. *Process Biochem.* **1999**, *34*, 451–465. [CrossRef]
84. Shahwan, T.; Erten, H.N. Temperature effects in barium sorption on natural kaolinite and chlorite-illite clays. *J. Radioanal. Nucl. Chem.* **2004**, *260*, 43–48. [CrossRef]
85. Langmuir, I. The adsorption of gases on plane surfaces of glass, mica and platinum. *J. Am. Chem. Soc.* **1918**, *40*, 1361–1403. [CrossRef]
86. Dada, A.O.; Olalekan, A.P.; Olatunya, A.M.; Dada, O. Langmuir, Freundlich, Temkin and Dubinin–Radushkevich Isotherms Studies of Equilibrium Sorption of Zn^{2+} Unto Phosphoric Acid Modified Rice Husk. *J. Appl. Chem.* **2012**, *3*, 38–45.
87. Mohmoud, A.; Rakass, S.; Oudghiri-Hassani, H.; Kooli, F.; Abboudi, M.; Ben Aouan, S. Iron Molybdate Fe_2 $(MoO_4)_3$ Nanoparticles: Efficient Sorbent for Methylene Blue Dye Removal from Aqueous Solutions. *Molecules* **2020**, *25*, 5100. [CrossRef]
88. Rakass, S.; Oudghiri-Hassani, H.; Abboudi, M.; Kooli, F.; Mohmoud, A.; Aljuhani, A.; Al Wadaani, F. Molybdenum Trioxide: Efficient Nanosorbent for Removal of Methylene Blue Dye from Aqueous Solutions. *Molecules* **2018**, *23*, 2295. [CrossRef] [PubMed]
89. Wu, T.; Cai, X.; Tan, S.; Li, H.; Liu, J.; Yang, W. Adsorption characteristics of acrylonitrile, p-toluenesulfonic acid, 1-naphthalenesulfonic acid and methyl blue on graphene in aqueous solutions. *Chem. Eng. J.* **2011**, *173*, 144–149. [CrossRef]
90. Fan, L.; Zhang, Y.; Luo, C.; Lu, F.; Qiu, H.; Sun, M. Synthesis and characterization of magnetic beta-cyclodextrin-chitosan nanoparticles as nano-adsorbents for removal of methyl blue. *Int. J. Biol. Macromol.* **2012**, *50*, 444–450. [CrossRef]
91. Zhang, F.; Lan, J.; Yang, Y.; Wei, T.; Tan, R.; Song, W. Adsorption behavior and mechanism of methyl blue on zinc oxide nanoparticles. *J. Nanopart. Res.* **2013**, *15*, 2034–2043. [CrossRef]
92. Li, L.H.; Xiao, J.; Liu, P.; Yang, G.W. Super adsorption capability from amorphousization of metal oxide nanoparticles for dye removal. *Sci. Rep.* **2015**, *5*, 9028. [CrossRef]
93. Maisa El Gamal, M.; Mousa, H.A.; El-Naas, M.H.; Zacharia, R.; Judd, S. Bio-regeneration of activated carbon: A comprehensive review. *Sep. Purif. Technol.* **2018**, *197*, 345–359. [CrossRef]
94. Yanlong Sun, Y.; Zhang, B.; Zheng, T.; Wang, P. Regeneration of activated carbon saturated with chloramphenicol by microwave and ultraviolet irradiation. *Chem. Eng. J.* **2017**, *320*, 264–270.
95. Erfan Sadatshojaei, E.; Esmaeilzadeh, F.; Fathikaljahi, J.; Barzi, S.E.H.S.; Wood, D.A. Regeneration of the Midrex Reformer Catalysts Using Supercritical Carbon Dioxide. *Chem. Eng. J.* **2018**, *343*, 748–758. [CrossRef]
96. Umapathy, V.; Neeraja, P.; Manikandan, A.; Ramu, P. Synthesis of $NiMoO_4$ nanoparticles by sol–gel method and their structural, morphological, optical, magnetic and photocatlytic properties. *Trans. Nonferrous Met. Soc. China* **2017**, *27*, 1785–1793. [CrossRef]
97. Ahmed, F.; Dewani, R.; Pervez, M.K.; Mahboob, S.J.; Soomro, S.A. Non-destructive FT-IR analysis of mono azo dyes. *Bulg. Chem. Commun.* **2016**, *48*, 71–77.
98. Etman, A.S.; Abdelhamid, H.N.; Yuan, Y.; Wang, L.; Zou, X.; Sun, J. Facile Water-Based Strategy for Synthesizing MoO3–x Nanosheets: Efficient Visible Light Photocatalysts for Dye Degradation. *ACS Omega* **2018**, *3*, 2201–2209. [CrossRef]
99. Aracena, A.; Sannino, A.; Jerez, O. Dissolution kinetics of molybdite in KOH media at different temperatures. *Trans. Nonferrous Met. Soc. China* **2018**, *28*, 177–185. [CrossRef]
100. Altenor, S.; Carene, B.; Emmanuel, E.; Lambert, J.; Ehrhardt, J.J.; Gaspard, S. Adsorption studies of methylene blue and phenol onto vetiver roots activated carbon prepared by chemical activation. *J. Hazard. Mater.* **2009**, *165*, 1029–1039. [CrossRef] [PubMed]